

# Journal of Materials Chemistry C

Accepted Manuscript



This is an *Accepted Manuscript*, which has been through the Royal Society of Chemistry peer review process and has been accepted for publication.

*Accepted Manuscripts* are published online shortly after acceptance, before technical editing, formatting and proof reading. Using this free service, authors can make their results available to the community, in citable form, before we publish the edited article. We will replace this *Accepted Manuscript* with the edited and formatted *Advance Article* as soon as it is available.

You can find more information about *Accepted Manuscripts* in the [Information for Authors](#).

Please note that technical editing may introduce minor changes to the text and/or graphics, which may alter content. The journal's standard [Terms & Conditions](#) and the [Ethical guidelines](#) still apply. In no event shall the Royal Society of Chemistry be held responsible for any errors or omissions in this *Accepted Manuscript* or any consequences arising from the use of any information it contains.

# Single-crystalline GeS nanoribbons for high sensitivity visible-light photodetectors

Changyong Lan, Chun Li\*, Yi Yin, Huayang Guo, Shuai Wang

State Key Laboratory of Electronic Thin Film and Integrated Device, and School of Optoelectronic Information, University of Electronic Science and Technology of China, Chengdu, 610054, China

**Keywords:** GeS; nanoribbons; visible light; photoresponse

## Abstract:

Single-crystalline GeS nanoribbons were synthesized by chemical vapor deposition for the first time. Structural characterization revealed that the nanoribbons grow along  $[0\bar{1}1]$  direction with thickness of 20~50 nm, width of several micrometers and length of hundreds of micrometers. The GeS nanoribbons show a p-type behavior verified from field effect transport measurement. The nanoribbon photodetectors respond to the entire visible incident light with response edge around 750 nm consistent with the band gap absorption of GeS. Strong nonlinear light-intensity-dependent response was observed between the measured illumination intensity from 0.25 to 212  $\mu\text{W}/\text{cm}^2$ . Under 530 nm light illumination, the maximum responsivity and external quantum efficiency are 139.9 A/W and 32730%, respectively. These results indicate that GeS nanoribbons are promising semiconducting nanomaterial for high performance broadband visible-light sensing applications.

---

\* Author to whom any correspondence should be addressed. E-mail: lichun@uestc.edu.cn

## 1. Introduction

Van der Waals type layered semiconductors have recently attracted wide attentions due to their analogous layered structure to graphene<sup>1</sup>. Among them, narrow band gap semiconductors, such as MoS<sub>2</sub>, WS<sub>2</sub>, GaS, GaSe, etc, offer promising optoelectronic properties for visible-light-absorbing components integrated in photodetectors, photovoltaic devices and photoelectrochemical cells<sup>2</sup>. As a compound semiconductor, the photo-electron conversion efficiency strongly relies on its crystallinity. Thanks to the tape-assisted micromechanical exfoliation from their layered bulk crystals, microscale single-crystalline flakes with few or multi-layer in thickness and microscale in width can be readily obtained. And intrinsic photoresponse properties can be subsequently investigated based on the photodetector fabricated by sophisticated electron beam lithography (EBL) technique. The high-crystallinity generally guarantees outstanding photoresponse performance. For example, the micromechanical exfoliated few layered GaS showed excellent photoresponse properties with photo-response of 64.43 A/W and external quantum efficiency (EQE) of 12621%<sup>3</sup>.

Although micromechanical exfoliation combined with EBL greatly accelerates the investigation of fundamental electrical and optoelectrical property of the layered semiconducting nanomaterials, high-yield and reproducible synthesis of those nanomaterial are highly desired from the application point of view. For layered materials, because of their layered crystal structural nature, two-dimensional (2D) planar growth is thermodynamically preferred<sup>4</sup>. However, one-dimensional (1D) nanostructures of those layered materials can be rationally synthesized in a highly anisotropic growth environment. Note that, in the past ten years, tremendous single-crystalline 1D semiconducting nanomaterials have been synthesized by the self-organized

crystal growth method<sup>5, 6</sup>. Recently, there are also many reports on the synthesis of layered semiconductor in 1D form<sup>7-10</sup>. They have been demonstrated as photodetectors with much improved photo-sensing performance compared with their polycrystalline film and bulk counterparts<sup>11</sup>. More importantly, these single-crystalline 1D photo-sensing nanomaterials are particularly interest for flexible photodetector<sup>8</sup>.

GeS, as a layered semiconductors with a distorted rock-salt orthorhombic structure<sup>14</sup> and a p-type semiconductor with a band gap of 1.65 eV<sup>12</sup>, is considered to be a photovoltaic material for solar cell<sup>13</sup>. Till now, various kinds of nanostructured GeS have been reported, such as nanosheets<sup>13</sup>, nanoflowers<sup>15</sup>, nanowire-nanosheet epitaxial structures<sup>16</sup>, and nanoparticles<sup>17</sup>. However, to the best of our knowledge no literature has been reported on the synthesis of single-crystalline 1D GeS nanomaterials. Furthermore, the photoresponse properties of nanostructured single-crystalline GeS have not been explored. Here, we reported the synthesis and photoresponse properties of single-crystalline GeS nanoribbons. The photodetectors based on GeS nanoribbons show high sensitivity and stability to visible light, which enable them to function at extremely low illumination intensities.

## 2. Experimental section

The nanoribbons were synthesized in a horizontal single-zone tube furnace. In a typical synthesis, a quartz boat loaded with 10 mg of GeS powder (99.99%, Sigma-Aldrich) was placed at the center of a quartz tube. Si substrates coated with 5 nm thermal evaporated Au film or coated with GeS microparticles were then placed downstream side from the furnace center. The quartz tube was evacuated to 0.1 Pa and subsequently flushed three times with high-purity Ar gas (5N).

After that, Ar gas with a flow rate of 50 sccm was introduced into the quartz tube and the pressure in the tube was maintained at 60 Torr. Then the temperature of the furnace was raised to 450 °C in 20 min and kept for 10 min. The corresponding substrate temperature was about 340 °C. After the deposition, the furnace was cooled to room temperature naturally.

The X-ray diffraction (XRD) patterns were recorded using a Rigaku X-ray diffractometer with a Cu  $K\alpha$  radiation source. The morphology and crystal structure of the products were analyzed by a JEOL-6400 field emission scanning electron microscope (SEM), and a JEOL-2010 transmission electron microscopy (TEM, operated at 200 kV), respectively. The thickness of the nanoribbons were measured using a Dimension 3000 atomic force microscope (AFM).

For device fabrication, the GeS nanoribbons were transferred to a SiO<sub>2</sub>/Si substrate by a physical dry transfer technique<sup>18</sup> which facilitate the nanoribbon alignment and eliminate the possible contamination induced from the solution in the conventional ultrasonic dispersion method. Standard photolithography technique was used to define contact electrodes with a gap width of 5 μm. A Ti (100 nm) film served as electrodes were deposited by e-beam evaporation. Monochromatic illumination was provided by a Zolix Omni-300 monochromator with a supercontinuum laser source (SC-Pro, Wuhan Yangtz Soton Laser). The illumination light power intensity was measured by a Newport 1954 power meter. The current-voltage ( $I$ - $V$ ) and the current-time ( $I$ - $T$ ) were recorded using an Agilent B2902A source unit in a home-made probe station.

### 3. Results and discussion

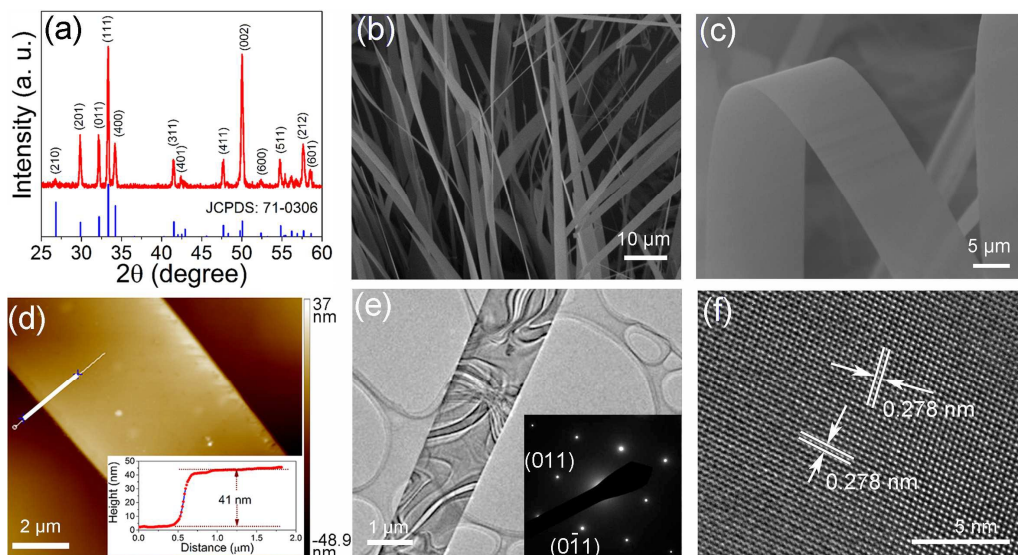


Figure 1. Structural characterization of the GeS nanoribbons. (a) XRD pattern of the as-grown product. The peaks are indexed according to orthorhombic structured GeS (JCPDS No. 71-0306). (b) and (c) SEM images of the GeS nanoribbons. (d) AFM image of a typical GeS nanoribbon transferred to the SiO<sub>2</sub>/Si substrate. The inset shows the height profile along the white line in the AFM image. (e) TEM image of a typical GeS nanoribbon. The inset shows a corresponding SAED pattern. (f) The corresponding HRTEM image of the nanoribbon showing in (e).

We found that without Au film or GeS microparticle coating, the products are only randomly orientated nanosheets<sup>15</sup>. With Au film or GeS microparticle coating, the nanoribbons can be obtained under above-mentioned growth conditions. The morphology and crystal structure of the as-grown nanoribbons are similar except the yield of nanoribbons grown on the Au thin film substrate is slightly higher than that grown on the microparticle coated substrate (See supporting information figure S1). Therefore, our structural characterization and device fabrication were

focused on the nanoribbons grown on Au thin film substrate. To determine the crystal structure of the product, XRD pattern of the product was measured and the result is shown in fig. 1a. All diffraction peaks can be indexed according to the orthorhombic structured GeS with lattice constants of  $a = 1.047$  nm,  $b = 0.4297$  nm, and  $c = 0.3641$  nm (JCPDS No. 71-0306). The morphology of the product was examined by SEM as shown in fig. 1b and 1c. The product consists of large quantities of nanoribbons. The width of the nanoribbons is several micrometers and the length is hundreds of micrometers. The thickness of the nanoribbons determined by AFM is found in the range of about 20~50 nm. A typical AFM image is shown in fig. 1d. The height profile (inset in fig. 1d) along the white line indicates that the nanoribbon has a thickness 41 nm. The typical TEM image of the nanoribbon is shown in fig. 1e. The corresponding selected area electron diffraction (SAED) is shown in the inset of fig. 1e. Clear diffraction spots can be seen, which suggest its good crystallinity. The corresponding high resolution TEM (HRTEM) image of the nanoribbon is shown in fig. 1f. Lattice spacing of 0.278 nm can be recognized and corresponds to the  $\{011\}$  family planes of the orthorhombic structured GeS. The typical nanoribbon growth direction was found along  $[0\bar{1}1]$ . Based on further detailed crystal structure characterization, we believe the growth of GeS nanoribbons can be rationally attributed to so-called vapor-solid (VS) rather than vapor-liquid-solid (VLS) mechanism (See supporting information figure S2).

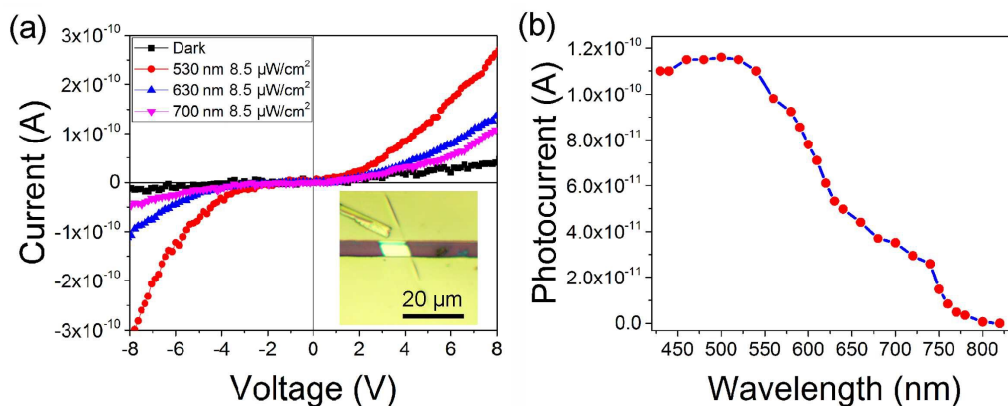


Figure 2. (a) Current *vs.* voltage (*I-V*) curves of the GeS nanoribbon photodetector with and without light illumination. (b) Photocurrent *vs.* wavelength. The bias voltage is 5 V and the light intensity is kept at  $8.5 \mu\text{W}/\text{cm}^2$  for each wavelength.

The CVD-grown 1D GeS nanoribbons with high crystallinity offer a good material platform for photo-detecting devices. To investigate its photoresponse properties, the performance of GeS nanoribbon photodetector working in photoconductive mode was measured. An optical image of the photodetector is shown in the inset of fig. 2a. To measure the photoresponsivity of the device, monochromatic light was used to perpendicularly illuminate onto the device surface and the corresponding current *versus* voltage (*I-V*) curves were recorded. The *I-V* curves of the photodetector exposed to incident light with different wavelengths and under dark conditions are shown in fig. 2a. The nonlinearity and asymmetry of the curves indicate a non-Ohmic contact between the Ti electrodes and the nanoribbon. Compared with the dark state, currents at the same bias voltage are higher under illumination, indicating that the device is photosensitive. In order to further investigate the wavelength dependent photoresponse, photocurrent as a function of wavelength was measured and the result is shown in fig. 2b. With the increase of wavelength, the photocurrent gradually decreases. The variation trend of photocurrent with wavelength is

consistent with the results in fig. 2a. As the wavelength approaches the band edge of GeS (1.65 eV<sup>12</sup>, corresponding to 750 nm), the photocurrent drops rapidly. Further increasing the wavelength, no detectable photocurrent can be observed. The illumination-wavelength-dependent photocurrent in vacuum exhibits same trend compared with that in air (See supporting information figure S3 )

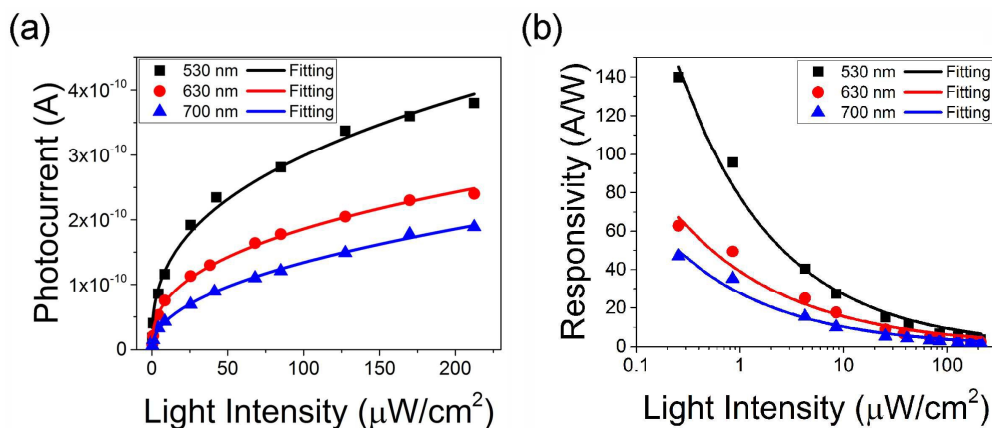


Figure 3. Photocurrent (a) and responsivity (b) of GeS nanoribbon photodetector as a function of illumination light intensity. The bias voltage is 5 V.

We also found that the GeS nanoribbon photoresponsivity shows strong nonlinear light-intensity-dependent characteristic. The photocurrent as a function of light intensity for wavelengths of 530, 630, and 700 nm is shown in fig. 3a. All these three curves are nonlinear and the curves can be fitted using the formula,

$$I_{\text{ph}} = \alpha P^{\beta} \quad (1)$$

where  $I_{\text{ph}}$  is photocurrent (A),  $\alpha$  is a coefficient,  $\beta$  is the exponent,  $P$  is the optical power (μW/cm<sup>2</sup>). Fitting of the curves resulted in  $I_{\text{ph}} = 5.51 \times 10^{-11} P^{0.367}$ ,  $I_{\text{ph}} = 3.16 \times 10^{-11} P^{0.385}$ , and  $I_{\text{ph}} = 1.52 \times 10^{-11} P^{0.472}$  for the wavelength of 530, 630, and 700 nm, respectively. We note that such nonlinear light-intensity-dependent property, i.e., the non-unity exponent, has also been observed

in many nanostructure-based photodetectors, such as ZrS<sub>3</sub> nanoribbons<sup>8</sup>, CdTe nanoribbons<sup>20</sup>, CuO nanowires<sup>21</sup>, In<sub>2</sub>S<sub>3</sub> nanowires<sup>22</sup>, which is a result of the complex processes of electron-hole generation, trapping, and recombination in the semiconductor<sup>23, 24</sup>.

Responsivity ( $R$ ) is an important parameter determining the detecting capability of a photodetector, which is defined as the photocurrent generated per unit power of incident light on the effective area of a photodetector. The  $R$  can be expressed as:

$$R = I_{\text{ph}} / \Phi \quad (2)$$

Here  $\Phi$  is the light power irradiated on the device and can be written as  $\Phi = PS$ , where  $S$  is the exposure area of the nanoribbons. The corresponding responsivity as a function of light intensity is shown in fig. 3b. As can be seen, lower light intensity gets higher responsivity. As the increase of light intensity, the responsivity drastically decreases. The maximum responsivities in our measurement are 139.9, 62.8, and 47.1 A/W for wavelength of 530, 630, and 700 nm, respectively. External quantum efficiency (EQE) is related to the number of electron-hole pairs excited by one absorbed photon, and is defined as

$$\text{EQE} = hcR / e\lambda \quad (3)$$

where  $h$  is Planck's constant,  $c$  is the velocity of light,  $e$  is the electronic charge, and  $\lambda$  is the exciting wavelength. According to the definition of EQE, EQE is proportional to  $R$  for a predefined excitation light. The maximum EQEs for the exciting light with wavelength of 530, 630, and 700 nm are 32730%, 12360%, and 8340%, respectively. These values are much higher compared with other 1D semiconductor detectors, such as HfS<sub>3</sub> nanoribbons<sup>9</sup>, In<sub>2</sub>Se<sub>3</sub> nanowires<sup>25</sup>. These results imply that our GeS nanoribbons are promising candidates for applications in high-selectivity and high sensitivity nanoscale photodetectors.

To elucidate the high reponsibility and distinctive nonlinear photoresponse, we measured field effect transport property of the as-grown GeS nanoribbon. The results indicate the GeS nanobelt is p-type semiconductor, which is consistent with bulk GeS [See supporting information figure S4]. The p-type behavior of GeS nanoribbon is consistent with the bulk GeS reported in literature, which can be attributed to the presence of Ge vacancies<sup>19</sup>. The high responsivity of GeS nanoribbon photodetector is likely to stem from combined effects of photocarrier multiplication inside the nanoribbon, carrier injection from the contacts, and surface states<sup>21</sup>. When the GeS nanoribbon is illuminated with incident light above its absorption band gap, photo-excited electron-hole pairs are generated and separated with external bias voltage. Therefore, additional electrons are made available for O<sub>2</sub> adsorption from the ambient. The photo-produced electrons participating in adsorption leave behind a paired hole that can contribute to the conduction process. In addition, the conduction bands raises due to the adsorption of O<sub>2</sub>, which draws in additional holes from the electrodes<sup>26</sup>. Therefore, the GeS nanoribbon photodetector exhibits higher responsivity at lower incident light intensity. The decrease of the responsivity at relatively high light intensity is primarily attributed to electron-trap saturation and increase of electron-hole recombination. As the traps are filled with electrons, the quasi-Fermi energy level rises, which leads to the increased number of free electrons in the system. As a result, the probability of electron-hole recombination increases at high illumination intensity.

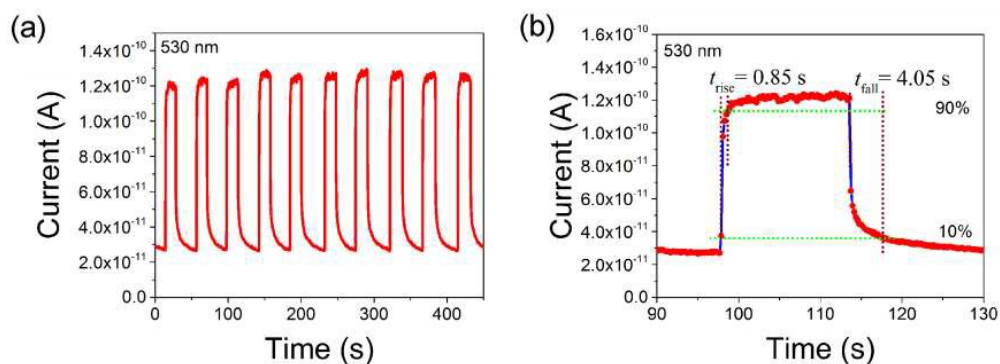


Figure 4. Time dependence of the GeS nanoribbon photodetector with bias voltage of 5 V under 530 nm light illumination ( $8.5 \mu\text{W}/\text{cm}^2$ ).

Repeatability and response speed are also key parameters for a photodetector. We measured the current of the device as a function of time under 530 nm light illumination with intensity of  $8.5 \mu\text{W}/\text{cm}^2$ . The results are shown in fig. 4. The switching behavior of the current with light on and off can clearly be observed. The on/off ratio of the current is 4.54. The reproducibility of the photocurrent suggests the high stability of the device. The magnified part of the current vs. time curve is shown in fig. 4b. The time needed for the current to increase from 10% to 90% of the peak value or vice versa is defined as the rise time and fall time, respectively. Hence, the rise time and the fall time can be determined to be 0.85 and 4.05 s, respectively. The time constant for the rise time is faster than the fall time, which indicates that charge carrier traps and defect states are involved in this process<sup>28</sup>.

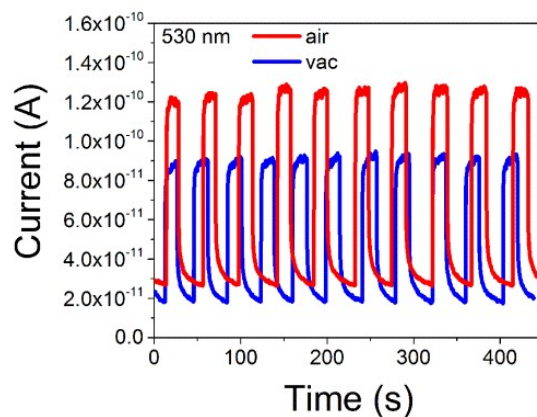


Figure 5. Current vs. time with chopped 530 nm light in air and in vacuum ( $1 \times 10^{-3}$  Pa). The light intensity and bias voltage is kept at  $8.5 \mu\text{W}/\text{cm}^2$ , 5 V respectively.

As a semiconducting nanomaterial with high surface-to-volume ratio and above-mentioned adsorbate-involved charge carrier generation, the surface adsorbate variation may influence the photoreponse. The environment sensitive photoresponse of 1D nanomaterials has been observed in many 1D nanostructures, such as  $\text{HfS}_3$  nanobelts<sup>12</sup>,  $\text{ZnO}$  nanowires<sup>26</sup>, etc. We measured the current-time curves with chopped 530 nm incident light in air and in vacuum to explore the working environment sensitive photoresponse of GeS nanoribbons. The measured results are shown in fig. 5. The dark current of the device in vacuum and in air is about  $1.78 \times 10^{-11}$  A and  $2.72 \times 10^{-11}$  A, respectively. The photocurrent in air is about  $9.87 \times 10^{-11}$  A, which is higher than that in vacuum ( $7.47 \times 10^{-11}$  A). The reduced photocurrent in vacuum can be attributed to the effect of removing of surface adsorbed  $\text{O}_2$  from a p-type semiconductor. In dark state, the adsorbed  $\text{O}_2$  can trap electrons so that the conduction band and valance band at the nanoribbon surface increase<sup>26</sup>. The increase of valance band leads to the increase of hole concentration near the surface. Since the adsorbed  $\text{O}_2$  is rare in vacuum, the dark current in vacuum should be smaller than that in air,

which is consistent with our result. As above-mentioned, the photo-generated electrons can be trapped by adsorbed  $O_2$ , leading to the increased photocurrent. Due to the rare adsorbed  $O_2$  in vacuum, the photocurrent in vacuum get smaller than that in air. Note that similar behavior has also been observed in other p-type nanostructured semiconductors, such as  $HfS_3$  nanoribbons<sup>9</sup>. And such phenomenon is different from that of n-type semiconductors, where the photocurrent get enhanced in vacuum compared with that in air<sup>26,27</sup>.

#### 4. Conclusion

Single-crystalline GeS nanoribbons were synthesized by chemical vapor deposition method for the first time. The structural characterization indicates that the GeS nanoribbons are single-crystalline and grow along  $[0\bar{1}1]$  direction. They have a thickness of 20-50 nm, a width of several micrometers with and a length of hundreds of micrometers. Electrical transport measurements verify that they have a p-type semiconducting behavior. The fabricated GeS nanoribbon photodetectors respond to the whole visible incident light with response edge around 750 nm. Under the illumination of 530, 630, and 700 nm light, the maximum responsivity are 139.9, 62.8, and 47.1 A/W, respectively. And the photoresponse shows strong nonlinear light-intensity-dependent. These results reveal that GeS nanoribbons are promising for potential application on visible-light selective photo-sensing devices.

#### Acknowledgements

This work was supported by the Foundation for Innovative Research Groups of the National Natural Science Foundation of China (grant no. 61421002), the Program for New Century

Excellent Talents in University (grant no. NCET-13-0092), the National Natural Science Foundation of China (grant no. 61106040 and no. 61475030), the State Key Laboratory of Electronic Thin Film and Integrated Device Program (no. KFJJ201408), and the Central University Basic Scientific Research Business Expenses (no. 2672013ZYGX2013J060 and no. 2672013ZYGX2013J061).

### References

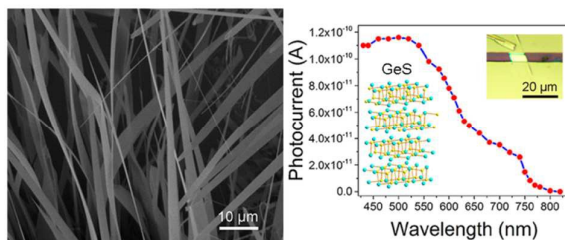
1. F. Xia, H. Wang, D. Xiao, M. Dubey and A. Ramasubramaniam, *Nat. Photonics*, 2014, **8**, 899-907.
2. A. Aruchamy, *Photoelectrochemistry and Photovoltaics of Layered Semiconductors*, Kluwer Academic Publishers, MA 02061, USA, 1992.
3. S. Yang, Y. Li, X. Wang, N. Huo, J.-B. Xia, S.-S. Li and J. Li, *Nanoscale*, 2014, **6**, 2582-2587.
4. L. Huang, Y. Yu, C. Li and L. Cao, *J. Phys. Chem. C*, 2013, **117**, 6469-6475.
5. L. Li, H. Lu, Z. Yang, L. Tong, Y. Bando and D. Golberg, *Adv. Mater.*, 2013, **25**, 1109-1113.
6. K. Deng and L. Li, *Adv. Mater.*, 2014, **26**, 2619-2635.
7. L. Li, X. Fang, T. Zhai, M. Liao, U. K. Gautam, X. Wu, Y. Koide, Y. Bando and D. Golberg, *Adv. Mater.*, 2010, **22**, 4151-4156.
8. Y. R. Tao, X. C. Wu and W. W. Xiong, *Small*, 2014, **10**, 4905-4911.
9. W.-W. Xiong, J.-Q. Chen, X.-C. Wu and J.-J. Zhu, *J. Mater. Chem. C*, 2014, **2**, 7392-7395.
10. W.-W. Xiong, J.-Q. Chen, X.-C. Wu and J.-J. Zhu, *J. Mater. Chem. C*, 2015, **3**, 1929-1934.
11. T. Zhai, X. Fang, M. Liao, X. Xu, H. Zeng, B. Yoshio and D. Golberg, *Sensors*, 2009, **9**,

6504-6529.

12. R. Eymard and A. Otto, *Phys. Rev. B*, 1977, **16**, 1616-1623.
13. D. D. Vaughn II, R. J. Patel, M. A. Hickner and R. E. Schaak, *J. Am. Chem. Soc.*, 2010, **132**, 15170-15172.
14. K. Bhatia, G. Parthasarathy and E. Gopal, *J. Phys. Chem. Solids*, 1984, **45**, 1189-1194.
15. C. Li, L. Huang, G. P. Snigdha, Y. Yu and L. Cao, *ACS Nano*, 2012, **6**, 8868-8877.
16. C. Li, Y. Yu, M. Chi and L. Cao, *Nano Lett.*, 2013, **13**, 948-953.
17. Y. J. Cho, H. S. Im, H. S. Kim, Y. Myung, S. H. Back, Y. R. Lim, C. S. Jung, D. M. Jang, J. Park and E. H. Cha, *ACS Nano*, 2013, **7**, 9075-9084.
18. L. Liao, Z. Zhang, B. Yan, Z. Zheng, Q. Bao, T. Wu, C. M. Li, Z. Shen, J. Zhang and H. Gong, *Nanotechnology*, 2009, **20**, 085203.
19. D. Bletskan, I. Madyar, S. Mikulaninets and M. Y. Sichka, *Inorganic Mater.*, 2000, **36**, 544-550.
20. X. Xie, S.-Y. Kwok, Z. Lu, Y. Liu, Y. Cao, L. Luo, J. A. Zapien, I. Bello, C.-S. Lee and S.-T. Lee, *Nanoscale*, 2012, **4**, 2914-2919.
21. B. J. Hansen, N. Kouklin, G. Lu, I.-K. Lin, J. Chen and X. Zhang, *J. Phys. Chem. C*, 2010, **114**, 2440-2447.
22. X. M. Xie and G. Z. Shen, *Nanoscale*, 2015, **7**, 5046-5052.
23. M. Shaygan, K. Davami, N. Kheirabi, C. K. Baek, G. Cuniberti, M. Meyyappan and J.-S. Lee, *Phys. Chem. Chem. Phys.*, 2014, **16**, 22687-22693.
24. R.-S. Chen, H.-Y. Chen, C.-Y. Lu, K.-H. Chen, C.-P. Chen, L.-C. Chen and Y.-J. Yang, *Appl. Phys. Lett.*, 2007, **91**, 223106.

25. T. Zhai, X. Fang, M. Liao, X. Xu, L. Li, B. Liu, Y. Koide, Y. Ma, J. Yao and Y. Bando, *ACS Nano*, 2010, **4**, 1596-1602.
26. C. Soci, A. Zhang, B. Xiang, S. A. Dayeh, D. Aplin, J. Park, X. Bao, Y.-H. Lo and D. Wang, *Nano Lett.*, 2007, **7**, 1003-1009.
27. C. Lan, C. Li, Y. Yin and Y. Liu, *Nanoscale*, 2015, **7**, 5974-5980.
28. K. Huang, Q. Zhang, F. Yang and D. He, *Nano Res.*, 2010, **3**, 281-287.

## Graphical abstract



Single-crystalline GeS nanoribbons were synthesized by chemical vapor deposition for the first time. The nanoribbon photodetectors respond to the entire visible incident light with response edge around 750 nm with high reponsivity, indicating its promising application for high performance broadband visible-light photo-detecting.